Profound analysis on sensing performance of Nanogap SiGe source DM-TFET biosensor

Mohammad K. Anvarifard[1], Zeinab Ramezani[2], I. S. Amiri[3,4,*] (iD), Khalil Tamersit[5,6], and Alireza Mahdavi Nejad[7]

[1] *Department of Engineering Sciences, Faculty of Technology and Engineering, East of Guilan, University of Guilan, Rudsar-Vajargah, Iran*

[2] *Department of Electrical and Computer Engineering, Northeastern University, Boston, MA 02115, USA*

[3] *Computational Optics Research Group, Advanced Institute of Materials Science, Ton Duc Thang University, Ho Chi Minh City, Vietnam*

[4] *Faculty of Applied Sciences, Ton Duc Thang University, Ho Chi Minh City, Vietnam*

[5] *Department of Electronics and Telecommunications, Université 8 Mai 1945 Guelma, 24000 Guelma, Algeria*

[6] *Laboratory of Inverse Problems, Modeling, Information and Systems (PIMIS), Université 8 Mai 1945 Guelma, 24000 Guelma, Algeria*

[7] *School of Engineering, Wentworth Institute of Technology, Boston, MA 02115, USA*

ABSTRACT

This present work is an extensive effort to report the key role of indispensable technical challenges in the sensing performance of an embedded nanogap SiGe source dielectric-modulated tunnel field effect transistor (SGS-DM-TFET) biosensor during the conjugation of biological samples for the first time. In order to reach high and brilliant insights into the different design considerations impacting on the sensing performance of the biosensor under the study, two key issues in terms of process-related issue and real-time-related issues covering biomolecules manners in the nanogap cavity of the biosensor have been comprehensively studied through extensive numerical simulation. Investigations in this work revealed that the SGS-DM-TFET biosensor must be truly configured for working in realistic conditions. The obtained results give us a useful guideline for sensing the biomolecules samples in the real conditions including low coverage percentage of biological samples, charge effect, and discrete probe position with the help of SGS-DM-TFET biosensor while keeping the high sensitivity.

Address correspondence to E-mail: irajsadeghamiri@tdtu.edu.vn

🙋 Springer

1 Introduction

Dielectric-modulated field effect transistor (DM-FET)-based biosensor [1–5] has obtained a great deal of interest in highly sensitive biomedical diagnostic tools since it can identify the biological samples without the process of labeling and making the biosensor high cost. It has high capabilities and reliability of FET-based structures that work in low power, analog/RF, and memory applications and it can also be used for sensing the biological samples [6–10]. Achieving a high sensitivity in the biosensors is very vital in biomedical different applications. Although the DM-FET-based biosensors are the attractive candidates owing to their high ON current at the event of sensing the biological samples, they give a weak sensitivity. Hence, the low biological density of samples can be led to a fault in the detection of samples [11, 12]. Hence, it is essential to develop the FET-based sensors to attain a high sensitivity. Tunneling FET structure (TFET) is considered as a promising candidate with low-leakage current and super-steep subthreshold swing in the solid-state devices [13, 14]. For that reason, the various resources have investigated the DM-TFET-based biosensor for low-power consumption label-free biomolecule detection aims since it presents a high sensitivity [15, 16].

In spite of all the advantages that the TFET biosensor provides for us, it suffers from a weak drain current when it is sensing the biological samples resulting in the reduction of signal-to–noise ratio (SNR). To overcome this serious weakness, a SiGe source dielectric-modulated TFET biosensor (SGS-DM-TFET) has been recently proposed to provide a good sensitivity along with relatively high current [17]. The reduction of bandgap energy and tunneling width are termed as the most important factors to promote the electrical performance of the SGS-DM-TFET biosensor. The SGS-DM-TFET biosensor has given a high sensitivity along with the enhanced drain current promising an excellent device in the biomedical applications. Although the proposal of the SGS-DM-TFET biosensor has led to the relaxation for researchers, its performance has not been investigated in the practical conditions, yet. This work, for the first time, focuses on the critical and more probable issues occurring during process and biomolecule detection steps. The process-related issue is the variation of nanogap cavity length and the real-time-related issues including the biomolecule behavior in the cavity in terms of the partial hybridization, charge effect, and discrete receptors/target biomolecules placement have been extensively investigated. This paper gives us a powerful insight into the SGS-DM-TFET biosensor sensing performance implemented in the real conditions thus successfully drawing an efficient guideline to select the optimum situation with respect to various and probable operating conditions.

It is worth noting that there are some interesting topics about the biosensors using the two-dimensional material such as graphene for detection of the DNA samples [18–21]. It is pointed out that we will only focus on materials based on the silicon.

2 Various SGS-DM-TFET biosensor schemes by practical issues

A double-gate (DG) DM-TFET structure with the embedded nanogap cavity at the source end has been utilized for the sensitivity analysis owing to steeper subthreshold swing and low-leakage current as illustrated in Fig. 1a.

The source region is filled by the material SiGe by germanium composition of 0.3 since this value has been selected as an optimum composition in the literature [17]. Also, the whole nanogap cavity is commonly filled by the air for pre-conjugation step measurement. The nanogap cavity thickness and length are considered to be 10 nm and 15 nm, respectively. Other essential parameters implemented in the simulation domain are listed in Table 1. The sensitivity of the biosensor is evaluated at the biased conditions $V_{ds} = 0.5$ V and $V_{gs} = 6$ V.

The methodology utilized for investigating the impact of partial hybridization (PH) of biological samples has been depicted in Fig. 1b–d. Figure 1b shows that the biomolecule is uniformly spread to the nanogap cavity by a 100% coverage percentage [15]. It is worth noting that Fig. 1c illustrates the uniform partial distribution of target samples in the cavity owing to the PH. In order to consider more realistic conditions, the non-uniform PH of biomolecule profile has been assumed as shown in Fig. 1d. This PH profile illustrates a ramp pattern by a gradual reduction of biomolecule thickness from the entrance of the cavity (end of the source) to the end of the cavity length. It is worth noting that only a part of the
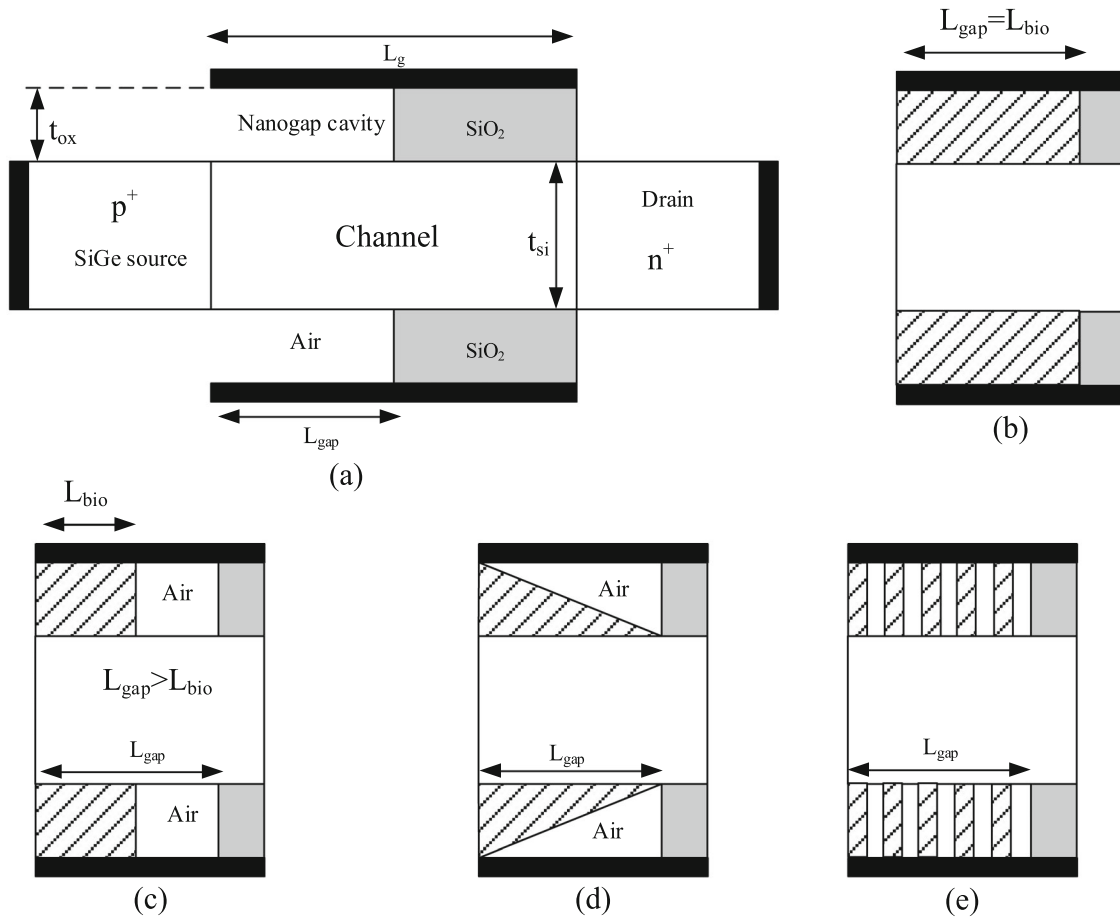
Fig. 1 a SGS-DM-TFET structure implemented in the simulation domain in the absence of the biomolecule. **b** Nanogap cavity is uniformly and completely filled by the biomolecule samples. **c** Nanogap cavity is uniformly and partially filled. **d** Nanogap cavity is non-uniformly and partially filled (ramp pattern). **e** Probes are embedded in discrete places inside the cavity [15]

Table 1 List of the SGS-DM-TFET biosensor parameters implemented in the simulation domain

Parameters	Values
Gate length, L_g	100 nm
Source/drain region length, (L_s, L_d)	50 nm
Gate oxide thickness, t_{ox}	10 nm
Nanogap cavity length, L_{gap}	15 nm
Silicon layer thickness, t_{si}	20 nm
Doping concentration of channel, N_a	1×10^{16} cm^{-3}
Doping concentration of source, N_a^+	1×10^{20} cm^{-3}
Doping concentration of drain, N_d^+	5×10^{18} cm^{-3}
Gate metal work function	4.1 eV

nanogap cavity is filled by the biomolecule and its density is gradually reduced along the cavity length in the practical conditions. Indeed, it has been proved that the atomic obstacles provided by already filled biomolecules prevent other biomolecules distributed along the nanogap cavity [22]. Hence, retarding the filled biomolecules inside the cavity causes the biomolecule thickness reduced along the nanogap cavity. Also, in order to consider more realistic conditions, Fig. 1e shows the position of the discreet probes replaced in the nanogap cavity. These probes are introduced to the nanogap cavity as a discrete entity occurring in the real conditions during processing the biosensor. Indeed, the biological samples are trapped by these probes and will form the hybridized probe/target configuration. It is pointed out that each of these configurations has the main role in the sensing performance of the SGS-DM-TFET biosensor that will be completely explained in section IV.

3 Governing equations in the SGS-DM-TFET biosensor

In order to understand the electrostatic behavior of the aforementioned biosensor, the robust physical models involved in the semiconductor basic equations are included in the simulation domain of the structure under the study before/after the conjugation of biological samples. Two main fundamental equations in terms of Poisson equation and carrier continuity equations are considered to simulate the SGS-DM-TFET biosensor in the following:

$$\nabla.(\varepsilon\nabla\psi) = -\rho \tag{1}$$

$$\partial n/\partial t = (1/q)\nabla.(\overrightarrow{J_n}) + G_n - R_n \tag{2}$$

$$\partial p/\partial t = -(1/q)\nabla.(\overrightarrow{J_p}) + G_p - R_p \tag{3}$$

where, in equations above, ψ is the electrostatic potential, ε is local permittivity, ρ is local space charge density including electron concentration n, hole concentration p, acceptor doping profile N_a, and donor doping profile N_d, J_n is the electron current density, J_p is hole current density, $G_{n,p}$ and $R_{n,p}$ are the rates for the process of generation and recombination.

Regarding the aforementioned fundamental frameworks for modeling the biosensor, the main transport equations named as drift–diffusion equations are solved for both the carriers to compute the current densities in the simulation domain according to the subsequent forms [22]:

$$J_n = qD_n\nabla n - qn\mu_n\nabla\psi - n\mu_n(KT_L\nabla(Lnn_i)) \tag{4}$$

$$J_p = -qD_p\nabla p - qp\mu_p\nabla\psi + p\mu_p(KT_L\nabla(Lnn_i)) \tag{5}$$

$$J_p = -q\mu_p p\nabla\phi_p, \quad J_n = -q\mu_n n\nabla\phi_n \tag{6}$$

$$n = n_i \exp(q(\psi - \phi_n)/KT_L) \tag{7}$$

$$p = n_i \exp\left(-q\left(\psi - \phi_p\right)/KT_L\right) \tag{8}$$

In order to consider the realistic conditions, the nonlocal quantum equivalent capacitance model for the SGS-DM-TFET biosensor is utilized to compute the tunneling rate across the semiconductor junctions. The term for including the nonlocal tunneling process is given in the subsequent form [24]:

$$J(E) = \frac{q}{\pi v}\iint T(E)[f_l(E + E_T) - f_r(E + E_T)\rho(E_T)dE_E dE] \tag{9}$$

It is worth mentioning that the summation of the current density for all the related energies is added to the current density at the junction grid point to include the tunneling current density, successfully. Also, Fermi–Dirac static has been considered for the approximation of the carrier's density. In addition to considering Eqs. (1)–(9), other important physical models in terms of normal electric field-dependent mobility, interface charge effect, doping-dependent bandgap narrowing, and strain effect have been contained in the simulation domain to accurately analyze the proposed SGS-DM-TFET biosensor electric performance.

The electron mobility as a factor defining the device conduction has a serious dependence on the normal (transverse) electric field. Moreover, the velocity of carries will start to be saturated when the electric field increases. Hence, the parallel electric field-dependent mobility considering the saturation velocity gives an accurate evaluation at modeling the biosensor. This model has been activated in the simulation. Due to the non-uniformity of interfaces, the dangling bonds will be formed creating the interface charges. In this paper, both the non-uniformity and biomolecule charge have been modeled by the interface charge. Also, doping-dependent bandgap narrowing is an important factor that can impact on the carrier transfer. This is the result of the impacting heavily doped material on the bandgap in the materials. Indeed, an increase in the doping concentration will decree the bandgap should be considered in the simulation.

All the aforementioned main equations are discretized in the simulation domain and introduced to the ATLAS package which is from the SILVACO family for extracting the electrical parameters modeling the sensing performance of the SGS-DM-TFET biosensor [23]. It is pointed out that two important boundary conditions in terms of the Neumann and Dirichlet have been applied in the simulation domain in order to solve the basic semiconductor equations, numerically.

4 Fundamental physics behind SGS-DM-TFET

This section is attributed to the fundamental physics involved in the SGS-DM-TFET structure for the enhancement of the sensing performance. Figure 1 shows that the source region of the TFET device has been replaced by the SiGe material. Two main events in terms of the reduced bandgap and reduced tunneling width are exhibited in the result of this configuration. The figure shows that when the biomolecule is inserted inside the nanogap, the channel region is modulated resulting in the final increase in the channel conduction.

To better understand this revolution, the energy band profile of the SGS-DM-TFET structure along the lateral channel has been illustrated for before/after the conjugation of the biomolecule in Fig. 2. The condition of the bias has been brought in the inset of the figure. It is seen in the figure when the biomolecule is hybridized, the tunneling width is reduced making the device more conductive since more electrons can tunnel from this barrier. In order to theoretically show the enhancement of the tunneling current, the tunneling current density is given as follows [24]:

$$J_t = \frac{\sqrt{2}q^3 m^{*1/2} \xi V_a}{4\pi^2 \eta^2 E_g^{1/2}} exp\left(\frac{-4\sqrt{2m^*}(E_g - \eta\omega)^{3/2}}{3q\eta\xi}\right) \quad (10)$$

where q is electron charge, m^* is the carrier effective mass, ξ is the maximum electric field, and E_g E_g 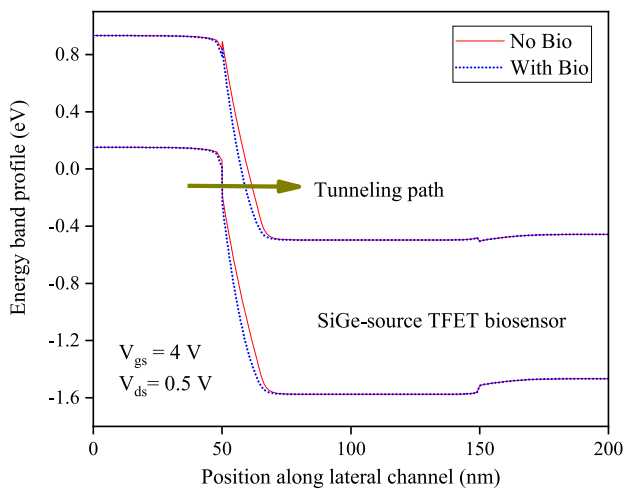is bandgap. The important parameters in the cases of effective mass, bandgap, and maximum internal electric field are design variables to maximize the current density. As we know, the SiGe material has less bandgap and tunneling mass compared to the silicon material. Hence, there is a good increase in the tunneling current of the SGS-DM-TFET structure.

For more clarification, the energy band profile of the hybridized TFET biosensor for both the Si and SiGe source materials is illustrated in Fig. 3. It is evident from the figure both the bandgap and the tunneling width of SiGe source TFET is far less than those of the Si source TFET. A meaningful result is an increase in the band-to-band tunneling (BTBT) generation rate for the SiGe source TFET relative to the Si source TFET as shown in Fig. 4.

5 Results and discussion

This section profoundly explains the role of the process-related issue and real-time-related issues in the sensitivity parameter of the SGS-DM-TFET biosensor. The partial hybridization (PH) of biological samples, charge effect, and discrete probe position inside the nanogap cavity are the important factors concerning the researchers about the electrical performance of the biosensor under the study which is explained in detail.

It is worth noting that the biosensor performance changes when a biomolecule sample enters the nanogap cavity. Hybridization of biomolecule samples on the probe receptors causes the dielectric constant of the material inside the nanogap cavity to
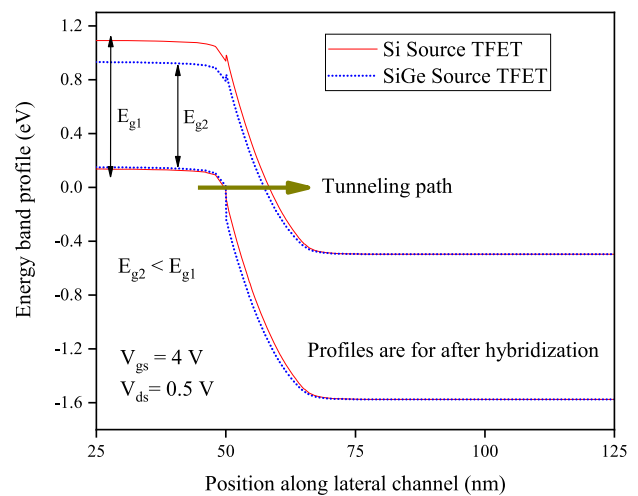
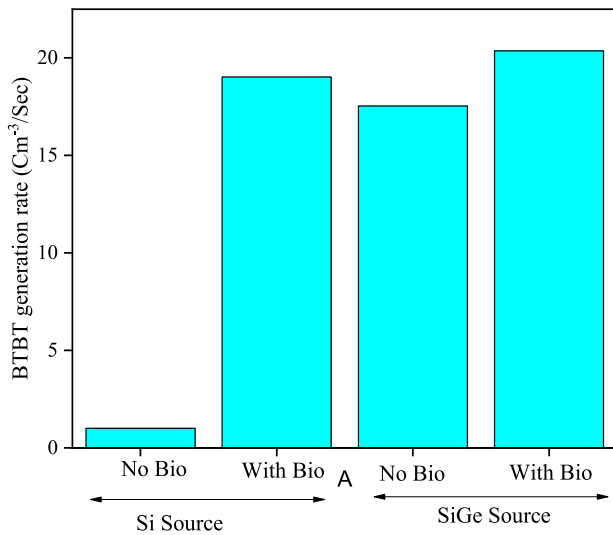Fig. 2 Energy band profile along the lateral channel

Fig. 3 Energy band profile along the lateral channel

Fig. 4 BTBT generation rate for SiGe and Si source TFET structures

vary from $K = 1$ (air material) to K_{bio} corresponding to a specific biomolecule. Unless otherwise stated, streptavidin–biotin binding system with $K_{bio} = 2.1$ is selected to evaluate the biosensor sensitivity throughout this paper. Actually, the conjugation of the biological samples inside the nanogap cavity modulates the channel electrostatic with a change in the channel carrier density. The band energy of the channel region is directed to fewer energies in the result of the introduced biomolecule conjugation thus providing massive tunneled carriers contributing to the conduction mechanism. Also, including the SiGe source will reduce the tunneling height and width to more promote the channel conduction.

A figure of merit in the case of $S_{bioTFET}$ which is based on the measurement of the drain current Ids at the applied bias $V_{ds} = 0.5$ V is defined to characterize the biosensor sensitivity. To reach this main variable, a general sensitivity parameter ($S_{current}$) is first extracted for the swept gate voltages as follows:

$$S_{current} = \left(I_{ds}^{bio} - I_{ds}^{no\_bio} \right) / I_{ds}^{no\_bio} \tag{11}$$

where $I_{ds}^{no\_bio}$ and I_{ds}^{bio} are termed as the drain current before ($K = 1$) and after ($K_{bio} = 2.1$) conjugation of biomolecules, respectively. Then, $S_{bioTFET}$ corresponding to maximum $S_{current}$, (which usually has a tendency into lower gate voltages) is given as the final sensitivity parameter of the biosensor for the sensing performance evaluation.

5.1 Effect of partial hybridization on sensing the performance

This subsection explains the influence of the PH biomolecules profiles on the SGS-DM-TFET biosensor sensitivity as depicted in Fig. 1. At first, the uniform PH impact for different biomolecule lengths (L_{bio}) varying from 50 to 100% of the nanogap cavity length (L_{gap}) has been investigated. The nanogap cavity length is set to the value of $L_{gap} = 15$ nm. To better understand the biosensor performance, the potential distribution along the channel surface has been plotted at the bias conditions $V_{gs} = 6$ V and $V_{ds} = 0.5$ V in Fig. 5.

As shown in the figure, the reduction of biomolecule coverage percentage from 100 to 50% of the nanogap cavity area leads to a decrease in the potential beneath the cavity. It is low coverage percent of biomolecule inside the cavity that reduces the dielectric modulation due to the enhanced effective gate oxide thickness. Hence, it is expected that the surface potential starts to decreases along the channel region thereby increasing the threshold voltage. A meaningful result is that the drain current will be reduced. The influence of the uniform PH biomolecule profile on the drain current of the biosensor is shown in Figs. 6 and 7.

The drain current as a function of the drain voltage and gate voltage has been demonstrated in the figures. It is obvious from the figures when the biomolecule coverage percentage is reduced, the drain current will be reduced resulting in the change in the
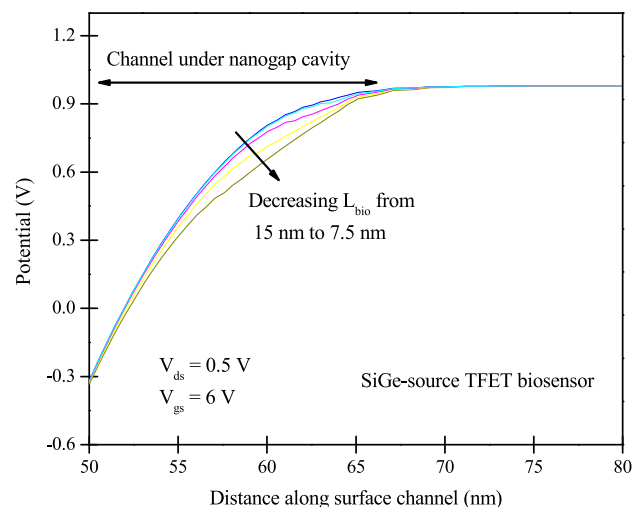

Fig. 5 Potential distribution along the surface channel for different L_{bio} ranged between 7.5 nm and 15 nm
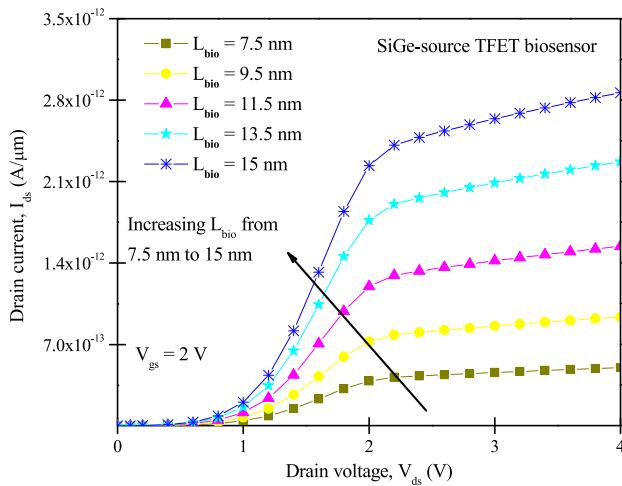
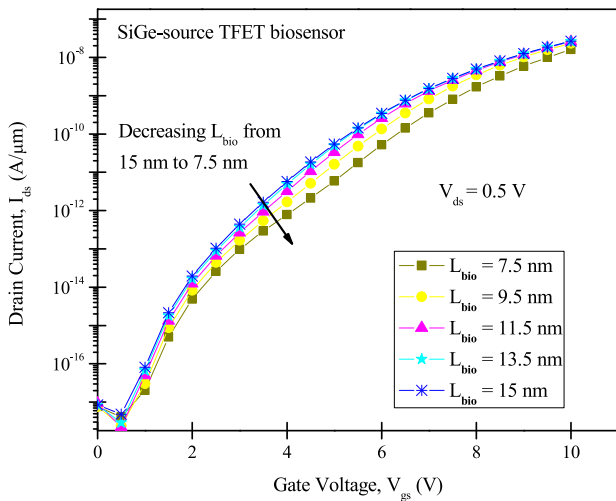**Fig. 6** Drain current as a function of the drain voltage for different L_{bio} ranged between 7.5 nm and 15 nm

Fig. 7 Drain current as a function of the gate voltage for different L_{bio} ranged between 7.5 nm and 15 nm

Fig. 8 Drain current sensitivity as a function of the gate voltage for different L_{bio} ranged between 7.5 nm and 15 nm

is due to the lowering of the conduction band energy of the channel, and the carriers which can tunnel more now. In order to more clarify, the sensitivity behavior of the figure can be explained by the behavior of the energy bands' edges at the region of nanogap. In fact, the bio-event-induced dielectric increment at the nanogap region alters the energy bands' edges at the level of L_{BIO} (in comparison to the initial state when the nanogap is uniformly filled by the air). Therefore, the increase in L_{BIO} dilates the modulation length of the concerned energy bands' edges leading to significant change in tunneling current, and hence, a higher sensitivity is recorded with L_{BIO} increasing, as shown in the same figure. Moreover, the record of maximum sensitivity at a specific gate bias shown at the same figure can be explained by the switching behavior of the proposed TFET device. As known, the biomolecules-induced dielectric increment alters the energy bands' edges at the nanogap level. Therefore, when this modulation is occurred at a gate bias near the off–on transition event (i.e., near the alignment between the source valence band-edge and the conduction band-edge underneath the gate [24], a significant change in drain current is obtained. Equivalently, the biomolecules will switch the proposed TFET device leading to a high current modulation while explaining the record of maximum sensitivity points in Fig. 8. It is worth indicating that this sensitive mechanism is valid for any DM-TFET-based nanobiosensor.

biosensor sensitivity. Also, it is clearly seen from the figures that a 50% biomolecule fill factor corresponding to L_{bio} = 7.5 nm creates a high subthreshold swing can affect on the SGS-DM-TFET sensing performance, adversely.

To predict the sensing performance of related biosensor, the drain current sensitivity ($S_{current}$) upon the gate voltage for the various biomolecule profiles with the uniform PH is illustrated in Fig. 8. In the studied biosensor, the source area has been replaced with heavily doping SiGe. Therefore, the tunneling width and the bandgap reduce which will increase the current. As can be seen in Fig. 8, as the gate voltage increases, the current sensitivity increases. It
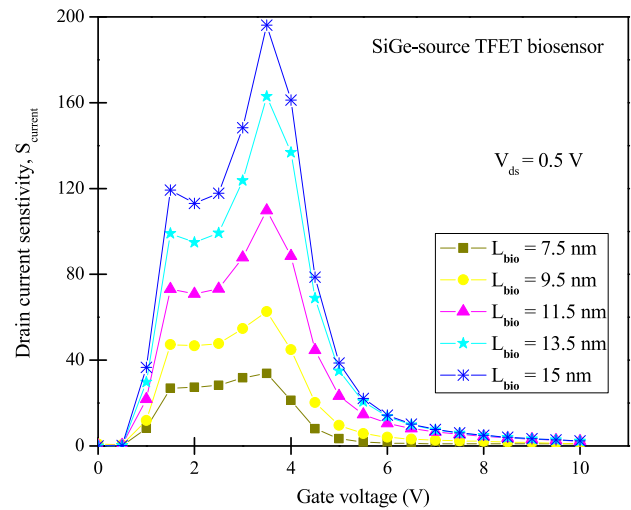
As shown in the figure, there is a local maximum for the curves of $S_{current}$ for each L_{bio}. The maximum value of $S_{current}$ defines $S_{bioTFET}$ for the SGS-DM-TFET biosensor as the final sensitivity parameter. For this reason, $S_{bioTFET}$ as a function of the filled region length by the biomolecule (L_{bio}) has been plotted in Fig. 9. It is evident from the figure that $S_{bioTFET}$ increases when L_{bio} increases. The SGS-DM-TFET biosensor obtains a good sensitivity for a fill factor of more than 60%. Also, the gate voltage where $S_{bioTFET}$ occurs has been shown in the inset of Fig. 9. A desirable and interesting result comprehended form the figure is achieving a fixed value of the gate voltage (3.5 V) needing to reach maximum drain current sensitivity ($S_{bioTEFT}$) at the event of the detection of biomolecule sample.

The effect of non-uniform PH including the different biomolecule profiles in terms of concave, convex, and ramp distribution (as illustrated in Fig. 10) has been inspected to analyze the sensing performance of the SGS-DM-TFET biosensor. These profiles are usually seen in real conditions.

It has been assumed that the different ramp profiles have the same biomolecule coverage area. Figure 11 shows $S_{bioTFET}$ for the related biomolecule profiles.

The concave and convex profiles include 5 steps with a length of 3 nm each. As shown in the figure, the concave profile gets the best sensitivity in the identification of the biomolecule sample followed by the convex profile and the ramp profile 10 nm to 0 nm, respectively. It was predictable that the
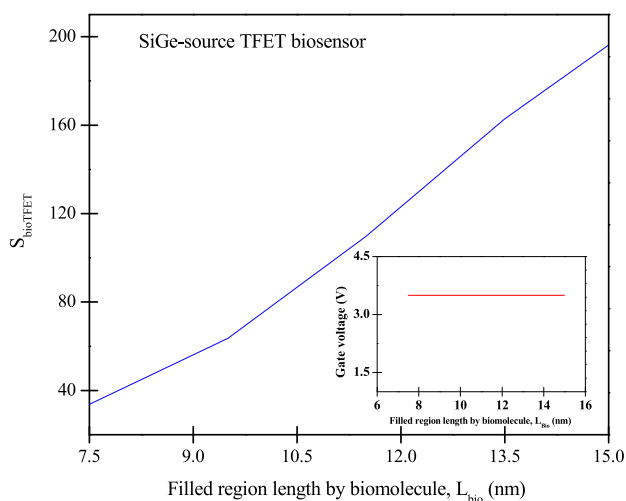
concave profile must present a maximum $S_{bioTFET}$ since the first step of the concave profile which is near the source/channel junction is completely filled by the biomolecule sample thus increasing the electrostatic modulation. Also, it is seen from the figure that $S_{bioTFET}$ is considerably reduced for the second, third, and fourth ramp profiles since the electrostatic coupling decrease for these arrangements. To have a deep intuition on the influence of uniform and non-uniform PH profiles, Table 2 lists $S_{bioTFET}$ along with the fill factor percentage of biological samples considering all the aforementioned biomolecule profiles that have ever been investigated. The nanogap cavity length has been set to a constant value of L_{gap} = 15 nm for all the biomolecule profiles in the table.

It is observed from the results that the highest sensitivity is attributed to the uniform PH with a 100% fill factor. Indeed, since the whole nanogap cavity space has been uniformly surrounded by the biomolecule sample, there will be a powerful coupling at the channel region thus increasing $S_{bioTFET}$. Moreover, the maximum sensitivity is not always obtained for a high fill factor percentage whereas it can effectively depend on the biomolecule profile near the source/channel junction. The compassion between the concave profile (78% fill factor) and the uniform PH (76.6% fill factor) shows that the concave profile gets a less sensing performance than the uniform PH profile. $S_{bioTFET}$ of uniform PH with a fewer fill factor is two times more than that of the concave profile. Because the effective gate oxide thickness for the concave profile is far more than that for the uniform PH at the nanogap cavity entrance resulting in the reduction of the dielectric modulation and sensitivity, too. Also, for the ramp biomolecule profiles having the identical fill factor percentage (50%), $S_{bioTFET}$ is not equal. The highest sensitivity is related to the ramp profile 10 to 0 nm (the first case) and the least sensitivity obtained for the ramp profile 7 to 3 nm. As depicted in Fig. 7, the ramp profile 10 to 0 nm has a less effective gate oxide thickness at near the source/channel junction (biomolecule thickness equals 10 nm in this point) as opposed to the ramp profile 7 to 3 nm whose the space of near the source/channel junction inside the nanogap cavity has been filled by both biomolecule and air (biomolecule thickness equals 7 nm in this point). Hence, it is concluded that both the biomolecule fill factor percentage inside the cavity and effective gate oxide thickness of the biosensor (biomolecule profile) have
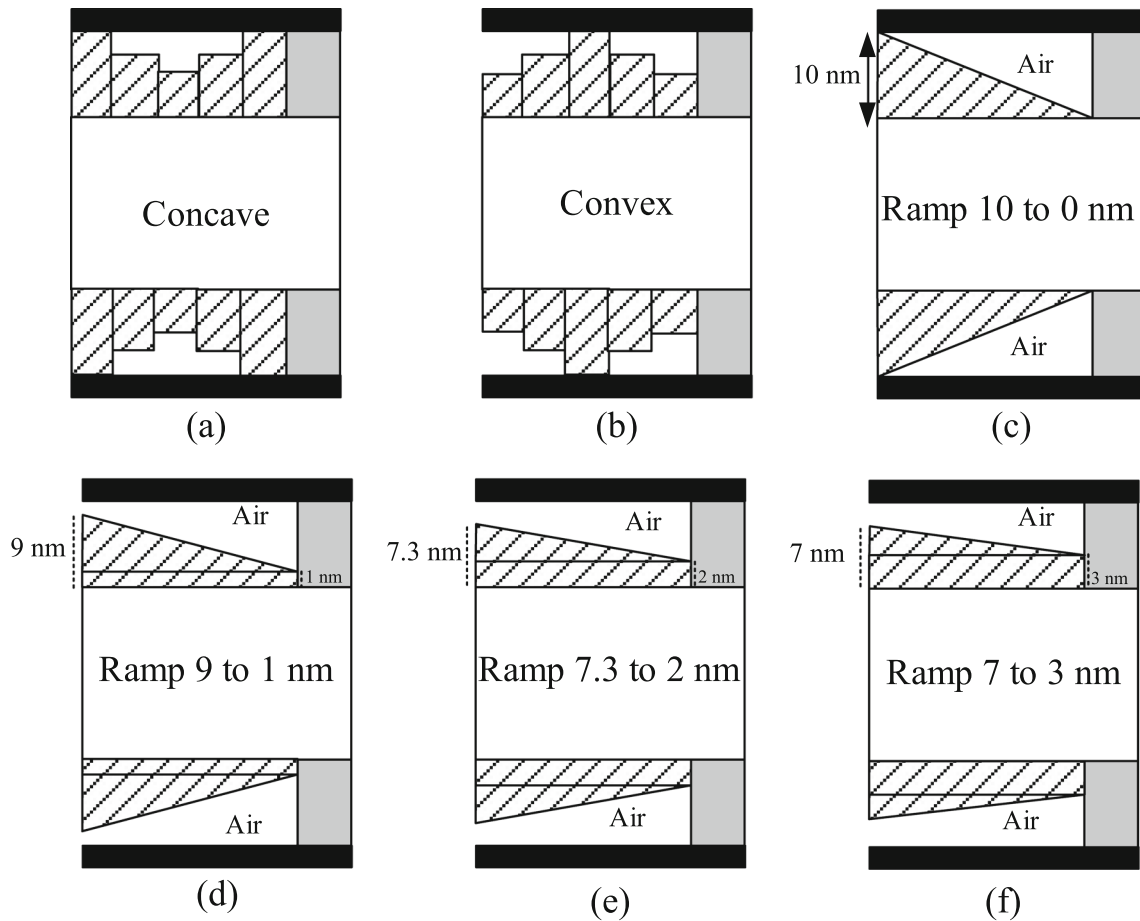

Fig. 9 $S_{bioTFET}$ as a function of the different L_{bio} ranged between 7.5 nm and 15 nm

Fig. 10 Various non-uniform and partial biomolecule profiles in terms of **a** concave profile **b** convex profile **c** ramp profile 10 nm to 0 nm **d** ramp profile 9 nm to 1 nm **e** ramp profile 7.3 nm to 2 nm **f** ramp profile 7 nm to 3 nm. It is worth noting that biomolecules coverage area inside the cavity is the same for ramp profiles [15]
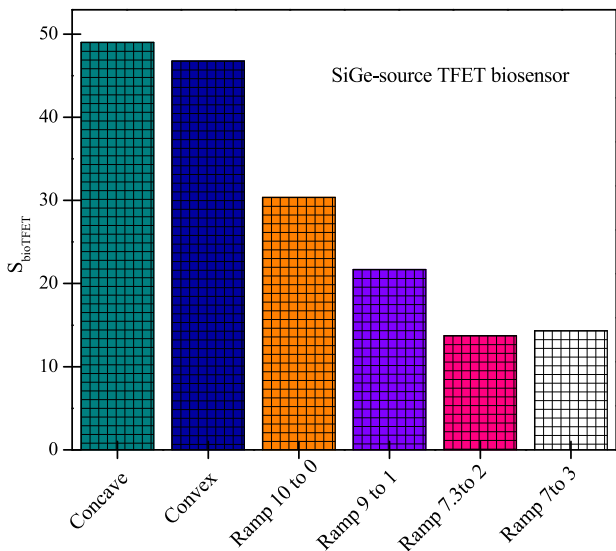

Fig. 11 S_{bioTFET} for the concave, convex, and different ramp profiles

a vital role in the sensing performance. Process-related complexities for the embedding of the nanogap cavity is one of the basic concerns can adversely impact on the sensing performance of the SGS-DM-TFET biosensor. To include this situation, Fig. 12 shows the sensitivity as a function of the nanogap cavity length changing from 10 to 50% of the physical gate length ($L_{\text{gap}} = \% L_{\text{g}}$).

It has been assumed to the biomolecule's hybridization is uniform and it is also completely filled inside the cavity. The results have been demonstrated for the gate lengths of 100 nm and 200 nm. It is evident from the figure that S_{bioTFET} increasers when the nanogap cavity length increases. As shown in the figure, the variation rate of the sensitivity for $L_{\text{gap}} = 200$ nm is far less than that for $L_{\text{gap}} = 100$ nm promising less sensitivity dependence of the biosensor on the scaling-down issue as compared to $L_{\text{gap}} = 100$ nm. Also, it can be stated that for

Table 2 Sensitivity and fill factor percent for uniform and non-uniform different biomolecule profiles with complete and partial hybridization

Case	Fill factor (%)	$S_{bioTFET}$
Uniform PH $L_{bio} = 15$ nm	100	196.2
Uniform PH $L_{bio} = 11.5$ nm	76.6	109.8
Uniform PH $L_{bio} = 7.5$ nm	50	33.8
Non-uniform concave profile	78	49
Non-uniform convex profile	68	46.7
Non-uniform ramp profile (10 nm to 0 nm)	50	30.4
Non-uniform ramp profile (9 nm to 1 nm)	50	21.7
Non-uniform ramp profile (7.3 nm to 2 nm)	50	13.7
Non-uniform ramp profile (7 nm to 3 nm)	50	14.3
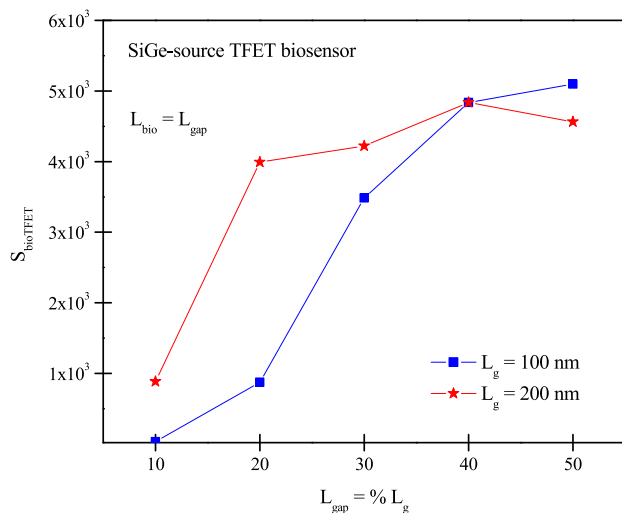
Fig. 12 $S_{bioTFET}$ upon the nanogap cavity length for $L_g = 100$ nm and 200 nm. The uniform and complete hybridization is assumed

Fig. 13 Gate voltage where $S_{bioTFET}$ is calculated upon the nanogap cavity length for $L_g = 100$ nm and 200 nm. The uniform and complete hybridization is assumed

the nanogap cavity lengths more than $20\%L_g$, the sensitivity experiences a calm variation for $Lg = 200$ nm whereas calm variation occurs for the nanogap cavity lengths more than $30\%L_g$ for $L_g = 100$ nm. Hence, it is expected that an increase in gate length leads to high select power for the creation of the nanogap cavity with no concern on process-related problems. Also, it can be fairly concluded that the concern about the dependence of sensitivity on the scaling issue can be removed for L_{gap} equal to $50\%L_g$ for various ranges of physical gate lengths. As the other investigation, the gate voltage where $S_{current}$ corresponds to $S_{bioTFET}$ has been illustrated as a function of the nanogap cavity length changing from 10 to 50% of L_g in Fig. 13.

It is observed from the figure, the gate voltage variation for $L_g = 200$ nm is far less than that for $L_{g-} = 100$ nm which is very desirable. Regarding Figs. 12 and 13, it can be stated that the gate voltage is
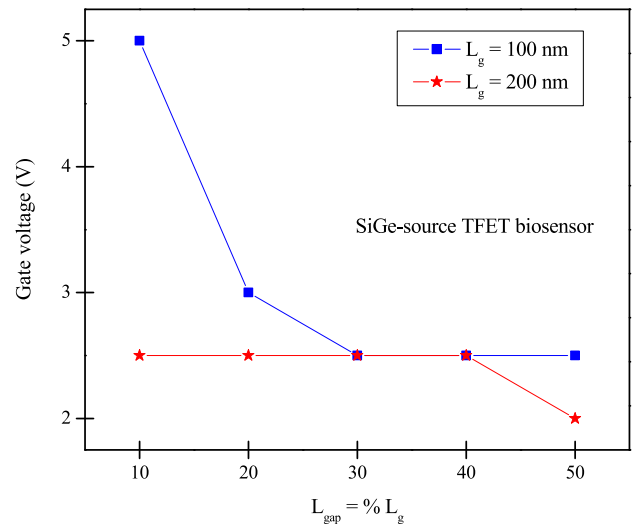
not an important problem for $L_{gap} \geq 30\%Lg$ for $L_{g-} = 100$ nm. Also, it is not an important issue for $L_{gap-} \geq 20\% L_g$ for $L_g = 200$ nm. It is worth noting that these interesting obtained results had already been explored for the sensitivity parameter as shown in Fig. 12.

5.2 Effect of biomolecule charge on sensing sensitivity the performance

Since the biomolecules are negatively charged samples as usual, then the charge role in the sensing performance of biosensor can be very important. Figure 14 has demonstrated the charge effect on the sensing performance of the SGS-DM-TFET biosensor for various values of biomolecule dielectric constant.

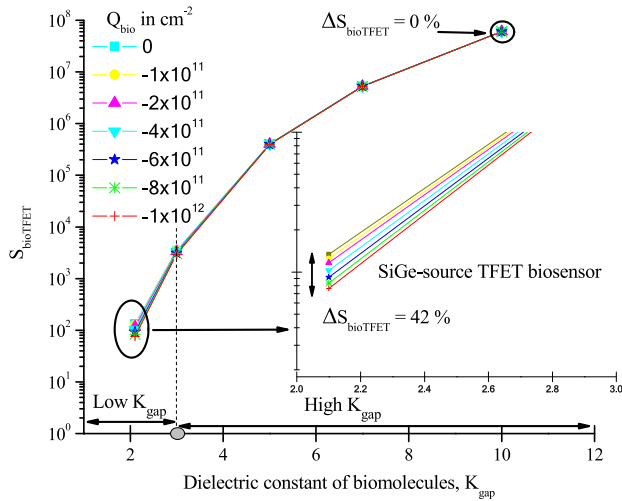Indeed, both the dielectric constant and charge amount of the biomolecule sample influence on the

Fig. 14 S_{bioTFET} as a function of the dielectric constants for the negatively charged biomolecules. The figure shows the low sensitivity variations

sensitivity of biosensor, simultaneously. As shown in the figure, the charge effect on S_{bioTFET} for the SGS-DM-TFET biosensor is not serious and it presents a weak dependence on the charge for the various dielectric constants. Moreover, the sensitivity is more spared for the charged biomolecules in K_{gap} less than 3 (low K_{gap} region) as shown in Fig. 14. To better conceive, a magnification of the sensitivity curve around small dielectric constants has been done and plotted in the inset of the figure. It is clear from the figure that the reduction rate of the sensitivity $\nabla S_{bioTFET}$ referenced by the natural biomolecule sample is only 42% for $K_{\text{gap}} = 2$ and is nearly 0% for $K_{\text{gap}} = 10$. As a general notation, it is stated that the SGS-DM-TFET sensing performance does not have important dependence on the biomolecule charges promising a high-reliable biosensor for the detection of various no-charged/charged biomolecules with no degradation on the sensitivity performance.

5.3 Effect of probe position on sensing the performance

Up to now, the distribution of biomolecules inside the nanogap cavity has been assumed to be a continuum for the better understanding of biosensor behavior. Moreover, the actual biomolecule binding is completely different. Because the probes and target biomolecules are embedded in discrete places as shown in Fig. 1e. In order to set this main and real issue, the hybridized probe and target with the

corresponded dielectric constant ($K_{\text{bio}} = 2.1$) are introduced into the nanogap cavity at definite discrete places forming rectangular shapes (slots) as an arrangement in Table 3. The gate length and the nanogap cavity length are 200 nm and 60 nm, respectively. The rectangular shapes have the height and width of 10 nm and 3 nm. It is worth noting that the shaded spaces show the absence of the biomolecule ($K = 1$).

The minimum and a maximum number of hybridized probes/targets pairs utilized for the detection are 4 and 16 as shown in Table. 3. In order to study the probe impact, eleven cases for placement of the probes have been predicted as shown at the table. It is seen from the table that the highest sensitivity is obtained for case 7 since the highest coverage percentage of the cavity by the biomolecule is related to it with an 80% fill factor. Also, the least sensitivity is related to case 11 since it includes the least fill factor by the biomolecule. Moreover, this is not the only reason why case 7 gives a high sensitivity. To better understand, a sensitivity comparison between case 4 (20% fill factor) and case 10 (25% fill factor) is performed. It is seen from the table that S_{bioTFET} for case 4 is more than that for case 10 while case 4 presents a less coverage percentage in comparison with case 10. Actually, the fill factor percentage of the biomolecule is not the only factor to improve the sensitivity. It is important to how to place the discrete hybridized probe/target pairs inside the nanogap cavity. Regarding case 1, the first hybridized probe is right at the source/channel junction (at the cavity entrance) whereas the first hybridized probe is displaced from the cavity entrance for case 2. Other procedures for biomolecule probe distribution are seen in the table showing different arrangements. Hence, it is stated that the electrostatic modulation on the channel region by biomolecules for case 4 is more than that for case 10 leading to a more sensitivity with a less biomolecule concentration. Hence, both fill factor percentage of biomolecules and placement of the hybridized probe and target pairs should be taken into consideration for reaching a desirable sensitivity. Hence, the biosensor design for reaching a good sensing performance leads to a trade-off between biomolecule concentration and placement of hybridized probe and target pairs which are very desirable.

The sensitivity fluctuations due to biomolecule distribution arranged in Table 3 have been

Table 3 Considered arrangements of hybridized probe/target pairs in discrete places investigating the probe impact on the sensitivity parameter [15]

Width of each slot= 3 nm, L_g = 200 nm, L_{gap} = 60 nm/ The shaded spaces show the absence of the biomolecule. / Biomolecule sample: ☆	Fill factor (%)	$S_{bioTFET}$
Case 1	50	205.7
Case 2	35	62
Case 3	25	33.7
Case 4	20	23.4
Case 5	70	1043.8
Case 6	75	1961.7
Case 7	80	2663.2
Case 8	50	207.2
Case 9	30	20.1
Case 10	25	5.2
Case 11	20	2.3

investigated over the covered areas percentage of the cavity by the biomolecule samples. Three covered ranges in the cases of 0–30%, 30–60%, and 60–90% are categorized as shown in Fig. 15a–c. Considering coverage percentage 0% to 30%, case 11 gives a minimum sensitivity due to reduced fill factor and displacement of a biomolecule from the source/channel entrance. Moreover, a comparison between case 3 and case 9 shows that the sensitivity of case 3 is more than that of case 9 in spite of including fewer biomolecule concentration.

Because the nanogap cavity for case 3 includes hybridized probe and target pairs right at source/channel junction whereas biomolecules are displaced from cavity entrance for the other case. One meaningful result is that the dielectric modulation of the biosensor increases leading to the improvement of sensing performance for case 3 as compared to case 9 having a more coverage percentage. Hence, case 3 can be taken as an optimum select for placement of probes to attain desirable sensitivity while it does not need high biomolecule density for detection. Regarding coverage percentage 30% to 60%, cases 1 and 8 are a proper candidate since they present a more biomolecule density. It is pointed out that the biomolecule density is dominated over the placement of the probe in case 8. But it is an inherent result and expectable. To perform a proper trade-off over

detectable sensitivity and minimum surface coverage percentage, case 2 is termed as optimum select. Regarding coverage percentage 60% to 90%, case 7 obtains the highest sensitivity by maximum fill factor percentage 80% followed by case 6 and case 5 which are an intuitive outcome.

Hence, it is concluded from the probe arrangement role investigation that cases 2 and 3 exhibit a decently high detectable sensitivity with minimum coverage surface density (35% and 20%, respectively) owing to proper placement of hybridized probe and target pairs leading to the formation of a powerful coupling at tunnel junction of the SGS-DM-TFET biosensor. This trade-off between coverage surface density of biomolecule and positioning the hybridized probes inside the cavity causes the SGS-DM-TFET biosensor to get a capability to effectively sense the biological samples with minimum surface coverage density applicable in biomedical applications.

The consideration of the asymmetry between the top cavity and back cavity in terms of nanogap filling can be a matter for further investigations in order to consider more complex biosensing scenarios. From optimization point of view, metaheuristic optimization techniques (e.g., genetic algorithms, particle swarm optimization, ant colony optimization, …etc.) [25] can be used in conjunction with the simulator to find the optimal values of physical, electrical, and
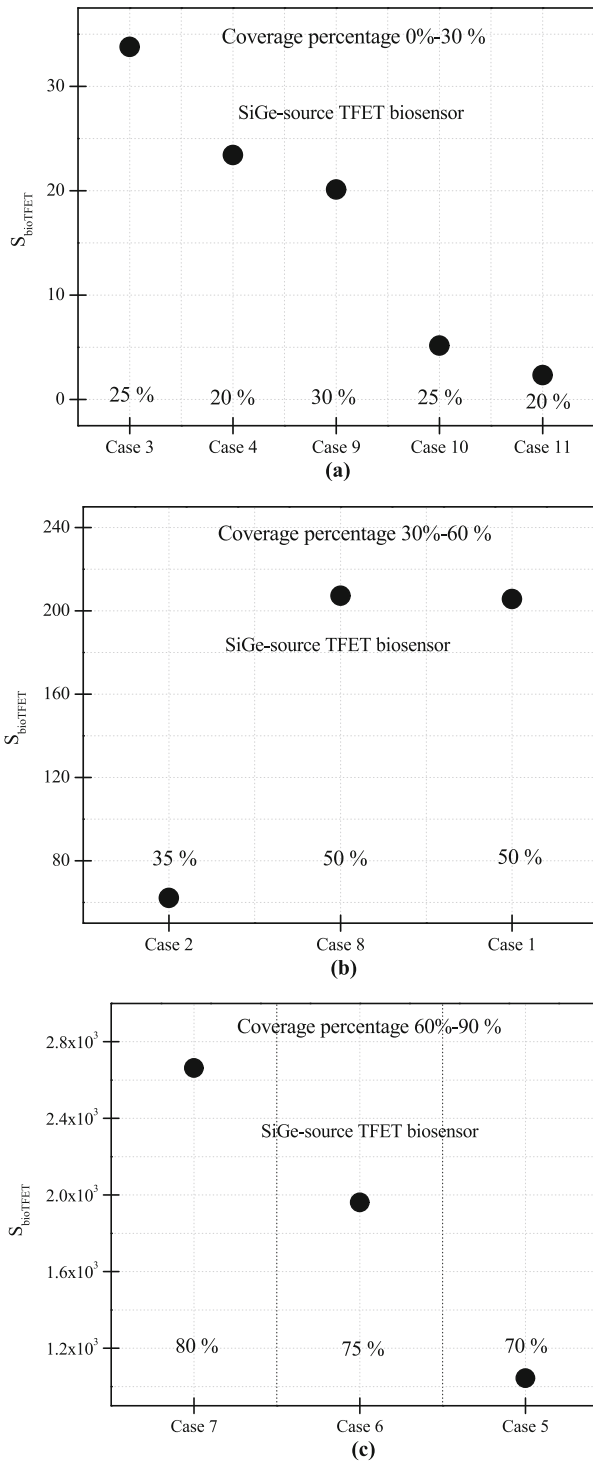
Fig. 15 $S_{bioTFET}$ for different cases modeling discreet probe placement with coverage percentages in terms of **a** 0–30% **b** 30–60% **c** 60–90%

6 Conclusion

The paper has extensively addressed process-related and real-time-related issues of the novel SGS-DM-TFET biosensor structure so as to investigate the vital sensing performance. The variation during the biosensor fabrication (change in the nanogap civility length), modifications during sensitivity evaluation (PH of biomolecules caused by atomic obstacles), and positioning the hybridized probe-target pairs in discrete places inside the nanogap cavity have been studied for the mentioned biosensor under dry ambient conditions. The extracted sensitivity which is one of the main parameters for evaluation of the sensing performance for the streptavidin–biotin binding system as a specific biomolecule showed that the SGS-DM-TFET biosensor can be implemented in the practical conditions without significant degradation on the sensing performance resulting in keeping the reliability. It has been observed from the explored results that the existence of biomolecule samples even at the small area inside the nanogap cavity can successfully modulate the channel electrostatic resulting in desirable and detectable sensitivity and also makes the biosensor more scalable. Also, the investigations explored that the charged biomolecules cannot influence on the sensing performance of the biosensor resulting in the mitigated sensitivity variation which is very favorable. The arrangement of probes inside the cavity (exploring case 2 and case 3 as an optimum select) revealed that the biosensor can reach an optimum and detectable sensitivity with the small amounts of biological samples which are proper for cost-effective biomedical diagnostics tools development.

References

1. S. Baoqing et al., A novel structure of silicon-on-insulator microring biosensor based on Young's two-slit interference and its simulation. J. Semicond. **32**(7), 074010 (2011)
2. P.R. Nair, M.A. Alam, Design considerations of silicon nanowire biosensors. IEEE Trans. Electron Devices **54**(12), 3400–3408 (2007)
3. H. Im et al., A dielectric-modulated field-effect transistor for biosensing. Nat. Nanotechnol. **2**(7), 430–434 (2007)

geometrical TFET parameters that lead to the extremely best sensitivity and scaling capability for high-performance label-free biosensing applications.

4. M.S. Parihar, A. Kranti, Enhanced sensitivity of double gate junctionless transistor architecture for biosensing applications. Nanotechnology **26**(14), 145201 (2015)

5. J. Luo et al., The influence of MBE and device structure on the electrical properties of GaAs HEMT biosensors. J. Semicond. **39**(12), 124007 (2018)

6. Y. Chen et al., An analytical drain current model for short-channel fully-depleted ultrathin silicon-on-insulator NMOS devices. Solid-State Electron. **38**(12), 2051–2057 (1995)

7. M. Saremi et al., A partial-SOI LDMOSFET with triangular buried-oxide for breakdown voltage improvement. Microelectron. Reliab. **51**(12), 2069–2076 (2011)

8. S.J. Mahabadi, S. Rajabi, J. Loiacono, A novel partial SOI LDMOSFET with periodic buried oxide for breakdown voltage and self heating effect enhancement. Superlattices Microstruct. **85**, 872–879 (2015)

9. M. Zareiee, A.A. Orouji, Superior electrical characteristics of novel nanoscale MOSFET with embedded tunnel diode. Superlattices Microstruct. **101**, 57–67 (2017)

10. A. Naderi, F. Heirani, Improvement in the performance of SOI-MESFETs by T-shaped oxide part at channel region: DC and RF characteristics. Superlattices Microstruct. **111**, 1022–1033 (2017)

11. R. Narang et al., A dielectric-modulated tunnel-FET-based biosensor for label-free detection: analytical modeling study and sensitivity analysis. IEEE Trans. Electron Devices **59**(10), 2809–2817 (2012)

12. R. Narang et al., Dielectric modulated tunnel field-effect transistor—a biomolecule sensor. IEEE Electron Device Lett. **33**(2), 266–268 (2011)

13. M.K. Anvarifard, A.A. Orouji, Evidence for enhanced reliability in a novel nanoscale partially-depleted SOI MOSFET. IEEE Trans. Device Mater. Reliab. **15**(4), 536–542 (2014)

14. R.M.I. Abadi, M. Saremi, A resonant tunneling nanowire field effect transistor with physical contractions: a negative differential resistance device for low power very large scale integration applications. J. Electron. Mater. **47**(2), 1091–1098 (2018)

15. R. Narang, M. Saxena, M. Gupta, Comparative analysis of dielectric-modulated FET and TFET-based biosensor. IEEE Trans. Nanotechnol. **14**(3), 427–435 (2015)

16. V. Nagavarapu, R. Jhaveri, J.C. Woo, The tunnel source (PNPN) n-MOSFET: A novel high performance transistor. IEEE Trans. Electron Devices **55**(4), 1013–1019 (2008)

17. S. Kanungo et al., Study and analysis of the effects of SiGe source and pocket-doped channel on sensing performance of dielectrically modulated tunnel FET-based biosensors. IEEE Trans. Electron Devices **63**(6), 2589–2596 (2016)

18. K. Tamersit, F. Djeffal, Carbon nanotube field-effect transistor with vacuum gate dielectric for label-free detection of DNA molecules: a computational investigation. IEEE Sens. J. **19**(20), 9263–9270 (2019)

19. K. Tamersit, F. Djeffal, Double-gate graphene nanoribbon field-effect transistor for DNA and gas sensing applications: simulation study and sensitivity analysis. IEEE Sens. J. **16**(11), 4180–4191 (2016)

20. M.K. Anvarifard, Z. Ramezani, I.S. Amiri, Proposal of an embedded nanogap biosensor by a graphene nanoribbon field-effect transistor for biological samples detection. Phys Status Solidi (A) **217**(2), 1900879 (2020)

21. M.K. Anvarifard, Z. Ramezani, I.S. Amiri, Label-free detection of DNA by a dielectric modulated armchair-graphene nanoribbon FET based biosensor in a dual-nanogap setup. Mater. Sci. Eng., C **117**, 111293 (2020)

22. A.W. Peterson, R.J. Heaton, R.M. Georgiadis, The effect of surface probe density on DNA hybridization. Nucleic Acids Res. **29**(24), 5163–5168 (2001)

23. S.I., *ATLAS User's Manual: 2-D Device Simulator* (S.I., Santa Clara, 2012)

24. K. Tamersit, Computational study of pn carbon nanotube tunnel field-effect transistor. IEEE Trans. Electron Devices **67**(2), 704–710 (2020)

25. K. Tamersit, M. Kotti, M. Fakhfakh, A new pressure microsensor based on dual-gate graphene field-effect transistor with a vertically movable top-gate: proposal, analysis, and optimization. AEU-Int. J. Electron. Commun. **124**, 153346 (2020)